Chinese Journal of Aeronautics, (2016), **xxx**(xx): xxx–xxx

Chinese Society of Aeronautics and Astronautics
& Beihang University

Chinese Journal of Aeronautics

cja@buaa.edu.cn
www.sciencedirect.com

FULL LENGTH ARTICLE

Drilling load modeling and validation based on the filling rate of auger flute in planetary sampling

Quan Qiquan *, **Tang Junyue, Yuan Fengpei, Jiang Shengyuan** *, **Deng Zongquan**

State Key Laboratory of Robotics and System, Harbin Institute of Technology, Harbin 150080, China

Received 1 February 2016; revised 14 March 2016; accepted 8 April 2016

KEYWORDS

Coring;
Drilling load;
Filling rate of auger flute;
Lunar regolith simulant;
Planetary drilling

Abstract Some type of penetration into a subsurface is required in planetary sampling. Drilling and coring, due to its efficient penetrating and cuttings removal characteristics, has been widely applied in previous sampling missions. Given the complicated mechanical properties of a planetary regolith, suitable drilling parameters should be matched with different drilling formations properly. Otherwise, drilling faults caused by overloads could easily happen. Hence, it is necessary to establish a drilling load model, which is able to reveal the relationships among drilling loads, an auger's structural parameters, soil's mechanical properties, and relevant drilling parameters. A concept for the filling rate of auger flute (FRAF) is proposed to describe drilling conditions. If the FRAF index under one group of drilling parameters is less than 1, this means that the auger flute currently removes cuttings smoothly. Otherwise, the auger will be choked with compressed cuttings. In drilling operations, the drilling loads on the auger mainly come from the conveyance action, while the drilling loads on the drill bit primarily come from the cutting action. Experiments in one typical lunar regolith simulant indicate that the estimated drilling loads based on the FRAF coincide with the test results quite well. Based on this drilling load model, drilling parameters have been optimized.

1. Introduction

As the Earth's closest nature satellite, the Moon completely records the 4.5 billion years evolutionary history of the solar system. Hence, when human beings started extraterrestrial explorations, the Moon definitely was the preferred target.[1,2] The main goal of lunar exploration is to understand the geological evolution of early stars through analyzing the subsurface composition beneath the surface. Compared with other sampling methods, drilling and coring, due to its efficient penetrating and cuttings removal characteristics, has been widely applied to past planetary sampling missions.[3,4]

* Corresponding authors.
E-mail addresses: quanqiquan@hit.edu.cn (Q. Quan), jiangshy@hit.edu.cn (S. Jiang).

Peer review under responsibility of Editorial Committee of CJA.

ELSEVIER Production and hosting by Elsevier

http://dx.doi.org/10.1016/j.cja.2016.05.003
1000-9361 © 2016 Production and hosting by Elsevier Ltd. on behalf of Chinese Society of Aeronautics and Astronautics.

At present, China is performing a lunar exploration program, namely the Chang'E project, the third phrase of which will use a hollow drill with a coring mechanism to capture the lunar soil and bring it back to the Earth.[5,6] According to reports on the lunar regolith, the lunar surface is largely covered by a layer of lunar regolith material. The vertical extension of this regolith layer is estimated to be of the order of several meters.[7] Because mechanical properties of the lunar regolith on different sampling spots or even at different depths on one spot can be quite different, the loads on a drilling device necessary to achieve penetration may often be unpredictable and this fact could seriously affect the stability of drilling. In terrestrial drilling, many types of detecting instruments are commonly used to accurately acquire geological information in order to assist real-time drilling. However, due to the mass and power constraints, such additional instrumentation can often not be implemented in planetary missions. For example, the lunar penetrating radar (LPR) that will be applied on the Chang'E missions, is not accurate enough to obtain the geological information on the lunar surface and near the subsurface that would be required for a safe drilling action.[8] Therefore, to reduce potential risks in penetrating, drilling loads should be monitored online and be reasonably restricted.

In a piercing process, cuttings in the annular region between the coring tube and the auger's outer surface are exerted by the cutting action by the cutting blade and are removed in the upward direction by the action, which is generated from the spiral auger and the borehole.[9] In the cutting and conveyance process described above, the sampling drill suffers reaction forces, generating drilling loads. Research on granular soil's spiral conveyance indicated that the cuttings' removal action affected drilling loads directly.[10] When a drill tool has penetrated to a certain depth, the driving power used for the cutting action becomes stable at some level, while the driving power needed for the conveying action increases dramatically and becomes the main power consumer[11].

To prepare for future Mars exploration, the University of California, Berkeley conducted a large number of experiments in sandstone cuttings under Martian conditions, revealing that an ice sublimation phenomenon generated by heating could effectively alleviate an auger's choking, greatly reducing the penetrating velocity and the drilling power.[12,13] According to the requirements of Chinese lunar exploration missions, the Harbin Institute of Technology analyzed the effects on the coring rate and the rotary torque by a drill tool's mechanical structure parameters and optimized the structural parameters.[14,15] It can be obviously concluded that to a specific sampling drill tool, suitable drilling parameters may efficiently reduce uncertain drilling loads.

Due to the restricted hardware resources on a planetary probe, drilling parameters should be reasonably optimized to reduce the drilling power needed for penetration. Establishing a drilling load model and revealing the relationships between the drilling load and the regolith's mechanical properties, will contribute to optimizing drilling parameters. The failure mode and conveyance state of the lunar regolith under a drill tool's action are theoretically analyzed in this paper. By using the FRAF index to describe the cuttings removal states of the lunar regolith, a drilling load model containing two typical drilling conditions has been established. Experiments in one typical lunar regolith simulant indicate that this drilling load model based on the FRAF coincides well with test results and can be used to optimize drilling parameters. Optimization indices of drilling parameters are analyzed according to the requirements of future lunar exploration. Based on the validated drilling load model, drilling parameters are optimized for application in lunar regolith simulants.

The remainder of this paper is organized as follows. One typical lunar regolith simulant and one potential drill tool are prepared firstly. The filling rate of the auger flute index is employed to describe the drilling conditions for different drilling parameters. The drilling load model established based on the FRAF index is validated for one typical lunar regolith simulant afterward. Finally, drilling parameters are optimized based on this drilling load model.

2. Lunar regolith simulant and drill tool

In many drilling applications, in particular in natural environments such as planetary surfaces, whose structure and layering are not known in advance, drilling loads have highly unpredictable and non-linear characteristics. Before establishing a drilling load model, a large number of drilling experiments should be carried out first for acquiring useful drilling state signals, which can serve as a sound basis for modeling. Both the structural parameters of the auger and the mechanical properties of the lunar regolith are expected to have considerable influences on the drilling performance. Therefore, in order to find an optimized set of drilling parameters suitable for application on a planetary lander mission, these influence factors need to be studied and evaluated in advance.

2.1. Lunar regolith simulant

Lunar regolith is a general term for the layer or mantle of fragmental rock material, formed by frequent meteoritic impacts on the atmosphere.[16] Studies of the returned samples indicate that the lunar regolith mainly contains five basic compositions: rock debris, mineral fragments, breccia, agglutinate, and glass-bonded aggregates.[7,17] The relative proportions of each composition, depending on the mineralogy of source rocks, vary from place to place, and even at different depths on one spot, they may be quite different. In order to verify our drilling load model, the lunar regolith simulant should mimic the mechanical properties of the real lunar regolith as close as possible.

In this paper, HIT-LS1# soil as shown in Fig. 1(a) has been chosen as the sampling material. The main component of HIT-LS1# soil is brown volcanic ash originating from the Jilin Province, China.[6] After the pressing process, the particle size distribution of this simulant varies from 1 μm to 100 μm, which is similar to that of the returned samples from the Apollo 17 landing site.[18] The density of HIT-LS1# soil is about 1.878 g/cm^3. According to the research by Heiken, among all mechanical properties, the shear strength of the lunar regolith, such as cohesion and internal angle, affects the drilling loads directly.[7] As shown in Fig. 1(b), under a repeated triaxle shear test, the shear strength of HIT-LS1# soil is acquired as follows: the average cohesion $c = 45.9$ kPa and the average internal friction angle $\varphi = 48°$. In this paper, the authors just consider the drilling interaction in a homogeneous lunar regolith. To acquire a homogeneous lunar regolith simulant for experimental validation, the lunar regolith simulant was compressed deliberately, which may result in a high cohesion.[19,20]. The

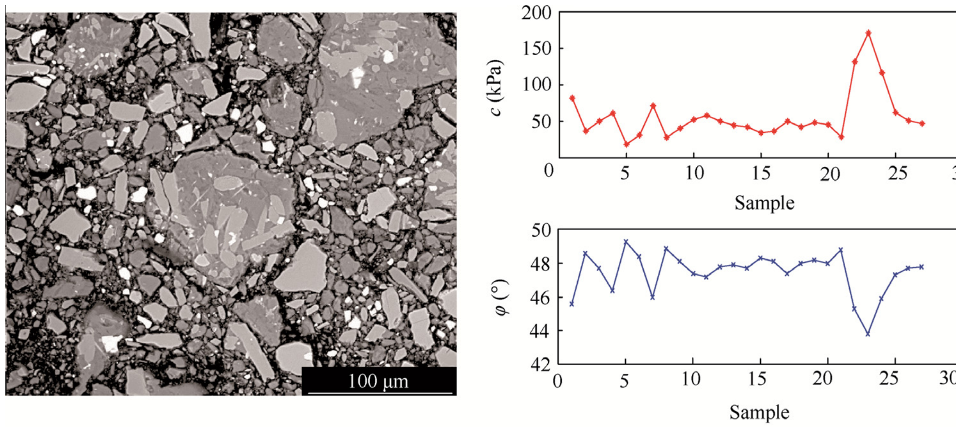

(a) Lunar simulant in electromicroscope

(b) Cohesion and internal friction angle

Fig. 1 One typical lunar regolith simulant: HIT-LS1# soil.

drilling experiments will be conducted based on this typical lunar regolith simulant.

2.2. Drill tool

The drill tool used in our experiments consists of a drill bit and a hollow auger. In this paper, a double-helix drill tool with double cutting blades is designed. The total length of this drill tool is approximately 0.5 m. There are two tungsten carbide cutting blades fixed to the drill bit matrix by a spotting weld process. To ensure that the cuttings can be removed from the auger flute fluently, the rake face of the cutting edge is aligned with the exit of the spiral auger flute. Taking the cuttings' removal effect and the drill bit's stress situation into account, the straight welded insert mode is adopted to install the cutting blades.[21] The rotary drill is designed as a split structure, in which the upper and lower bodies are connected by a trapezoidal thread. Former drilling experiments have shown that this double-helix drill tool has a good cutting performance and allows to remove cuttings ranging from granular regolith to hard rock quite well. Hence, the drilling load modeling in this paper will be based on this type of drill tool. To analyze the effects of various drilling parameters and the lunar regolith's mechanical parameters on the drilling load, the structural parameters of this drill tool are defined in Fig. 2 and listed in Table 1.

2.3. Flexible tube coring method

In a drilling process, the drill tool is driven by a rotary and percussive driving mechanism and a penetrating mechanism to pierce into the regolith. Inside the auger, there is an elaborately designed flexible tube coring mechanism, as shown in Fig. 3. There is a set of coring tubes inside the rotary auger, including a rigid tube and a flexible tube. The flexible tube is arranged between the auger and the rigid tube. One tip of the flexible tube is a sealing mechanism and the other tip is fixed on the connection component, connected with a dragging wire.

Once the drill bit contacts the planetary surface under the penetrating velocity v_p, one tip of the dragging wire will be fixed at a point on the probe. Moreover, the wire keeps a tense state in the whole penetrating process. The rigid tube moves downward with the auger synchronously, however, it does not rotate. When drilling into the regolith, the flexible tube begins to wrap the cutting core under the winding speed v_w. Since there is no relative locomotion between the flexible tube

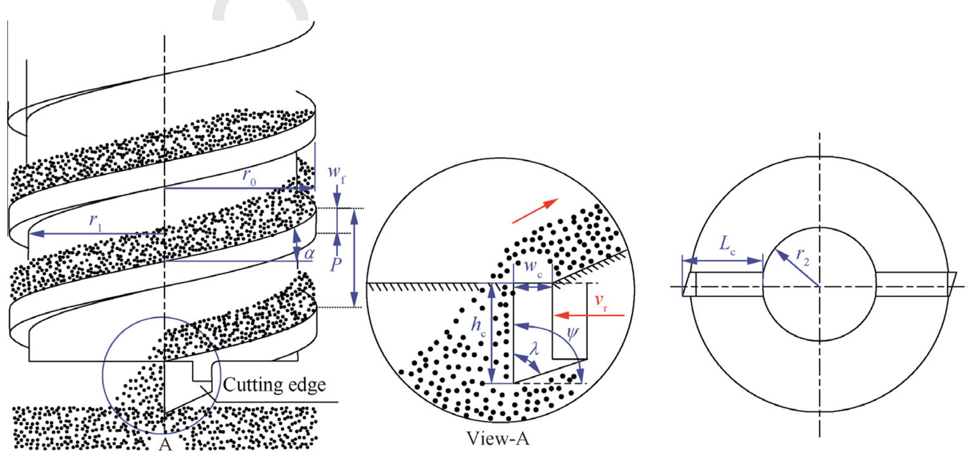

Fig. 2 Definition of the drill tool's structural parameters.

Table 1 Structural parameters of the drill tool.

Structure parameter	Value
Pitch, P (mm)	12
Helix angle, α (°)	13.4
Spiral flute thickness, w_f (mm)	3
Outer radius of auger, r_0 (mm)	16
Inner radius of auger, r_1 (mm)	15
Height of cutting blade, h_c (mm)	16
Thickness of cutting blade, w_c (mm)	3
Cutting angle, ψ (°)	90
Wedge angle, λ (°)	65
Length of cutting blade, L_c (mm)	9
Inner radius of drill bit, r_2 (mm)	7

and the core, this coring method can keep the original stratification of planetary soil. When the desired drilling depth is reached, the sealing tip at the end of the flexible tube will be activated to collect the soil sample into the closed space.

2.4. Planetary drilling & coring test-bed

To validate the drilling load model, the authors of this paper developed a planetary drilling and coring test-bed (PDCT), as shown in Fig. 4. The PDCT mainly consists of a bed frame, a lunar soil container, the drill tool, the penetrating drive unit, the rotary-percussive drive mechanism (RPDM), and the gravity compensation.[22,23]. A torque sensor is mounted on the output side of the rotary motor in order to monitor the rotary torque that the drill tool sustains, and an F/T sensor is installed on the bottom of the lunar soil container to monitor the penetration resistance force. Finally, on one side of the vertical rails, a magnetic scale displacement sensor is mounted to monitor the penetration velocity of the drill tool during the piercing process. To acquire the drilling loads online in drilling experiments, the data acquisition system of this test platform is based on xPC Target in MATLAB.

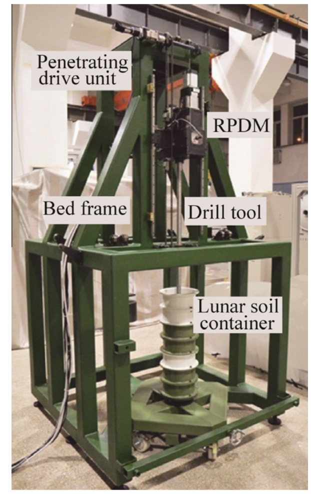

Fig. 4 Planetary drilling and coring test-bed.

3. Conveyance mechanism

Under the complex motions of rotation and penetration, cuttings are immediately removed from the bottom of the borehole. This removal principle is similar to that of a screw conveyor.[24,25] Referring to the spiral transport theory, the driving force for upward removal of the lunar regolith along the spiral auger mainly contains the following two aspects: the thrust exerted by the bottom of the borehole and the friction exerted by the wall of the borehole.

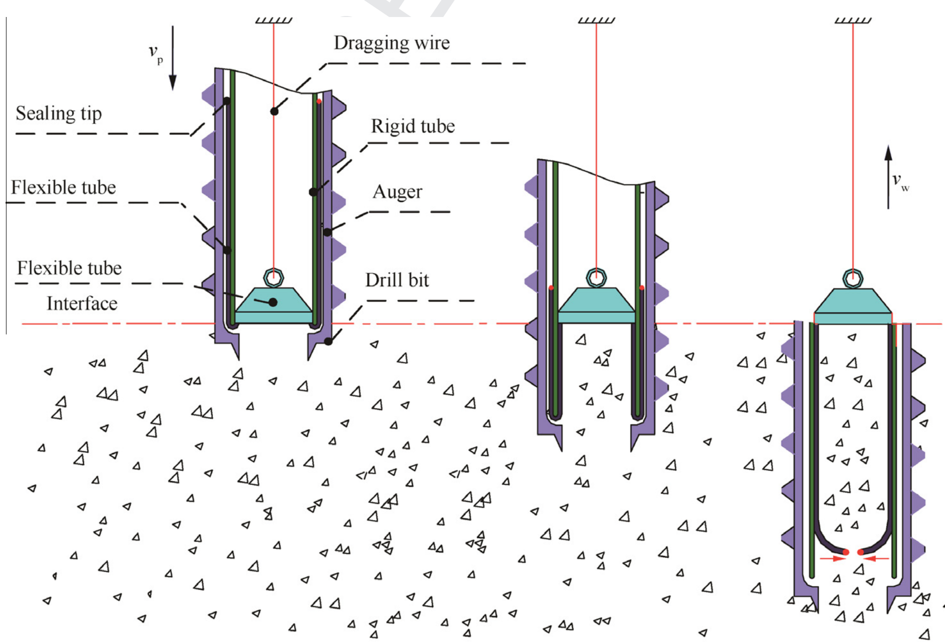

Fig. 3 The flexible tube coring method.[5]

Please cite this article in press as: Quan Q et al. Drilling load modeling and validation based on the filling rate of auger flute in planetary sampling, *Chin J Aeronaut* (2016), http://dx.doi.org/10.1016/j.cja.2016.05.003

3.1. Thrust from the bottom of the borehole

Because the lunar regolith becomes loose and granular after the cutting action by the drill bit, the conveyance analysis will mainly be focused on the granular regolith, assuming that there is a homogeneous granular regolith on the smooth ramp with an inclination angle α, which is the same as the helix angle in Table 1. The lunar soil sustains the thrust F_p from the bottom of the borehole, which causes an upward movement of the material along the ramp. The weight of lunar regolith of a thickness of 1, a length of L, and a height of s along the ramp direction is $\rho g_\mathrm{m} s \sin\alpha$. According to Rankine passive earth pressure theory,[26] the maximum thrust acting on the lunar soil can be calculated as follows:

$$F_{\mathrm{p_{max}}} = \frac{1}{2}\left(\frac{1+\sin\varphi}{1-\sin\varphi}\right)\rho g_\mathrm{m} s^2 \tag{1}$$

where ρ is the density of the granular soil and g_m is the acceleration of gravity on the moon. The static equilibrium equations are given as follows:

$$\rho g_\mathrm{m} s L \sin\alpha \leqslant \frac{1}{2}\left(\frac{1+\sin\varphi}{1-\sin\varphi}\right)\rho g_\mathrm{m} s^2 \tag{2}$$

Herein, $L\sin\alpha = H$, where H is the vertical height of the granular regolith. Incorporating H into the above equation and simplifying it, we obtain:

$$H \leqslant \frac{1}{2}\left(\frac{1+\sin\varphi}{1-\sin\varphi}\right)s \tag{3}$$

According to Eq. (3), the vertical height H of the granular regolith is controlled by the regolith's internal angle φ and height s. As shown in Fig. 5, when keeping the height of regolith in the spiral flute constant, H increases with the inner angle. Due to the fact that s is restricted by the drill pitch P and the blade thickness of the spiral flute h_c, the maximum height will be $P - h_\mathrm{c}$. For the designed double-helix drill tool and the compacted lunar regolith, the calculated maximum height of the lunar regolith is only about 9 mm.

Under a non-choking condition, there is no additional stress on the soil and the thrust from the bottom of the borehole can only push the lunar regolith over a limited distance. Therefore, it can be concluded that the thrust from the bottom of the borehole is not the main driving force for cuttings' removal under a non-choking condition. However, under a choking condition, an additional stress occurs, which can enhance the thrust from the bottom of the borehole and should be considered in modeling.

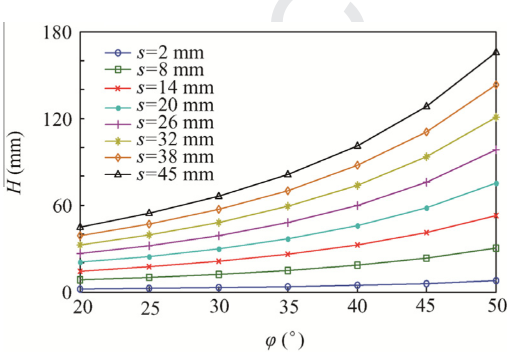

Fig. 5 Vertical height by the thrust from the bottom of the borehole.

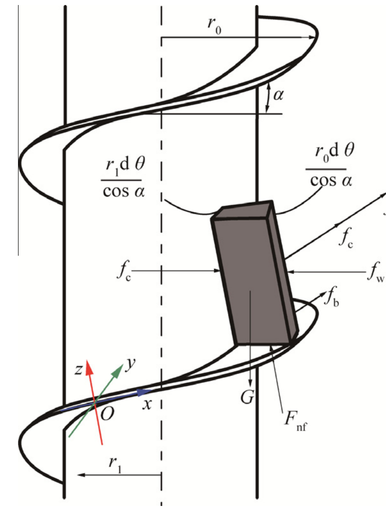

Fig. 6 Force analysis under the active earth pressure.

3.2. Friction from the wall of the borehole

The friction along the wall of the borehole is generated by the positive pressure acting on the wall. For the granular regolith in the spiral flute, the main positive pressure stems from the following three aspects: the active earth pressure, the centrifugal force, and the additional stress. In the following, three positive pressures will be discussed.

Consider a sector element of the lunar regolith on the flute ramp, of which the height of the lunar regolith element is s. As shown in Fig. 6, the Cartesian coordinate system O-xyz for force and motion analysis is built on the surface of the spiral flute, where F_c is the reaction force on the cylindrical surface of the auger, F_w is the reaction force on the wall of the borehole, F_nf is the supporting force on the bottom of the flute, and G is the gravity of the lunar regolith element.

According to the active earth pressure theory, the positive pressure acted on the lunar regolith σ_y at a drilling depth h is calculated as follows:

$$\sigma_y = \left(\frac{1-\sin\varphi}{1+\sin\varphi}\right)\sigma_z = \left(\frac{1-\sin\varphi}{1+\sin\varphi}\right)\rho g_\mathrm{m} h\cos\alpha \tag{4}$$

By analyzing the force states of a lunar regolith element, the resistances on the wall of the borehole f_w, at the bottom of the spiral flute f_b, and on the ceiling of the spiral flute f_c can be acquired:

$$\begin{cases} f_\mathrm{w} = \mu_\mathrm{w}\cdot F_\mathrm{w}\cos\alpha = \mu_\mathrm{w}\left(\frac{1-\sin\varphi}{1+\sin\varphi}\right)\frac{\rho g_\mathrm{m} s^2 r_0 \mathrm{d}\theta\cos\alpha}{2\cos\alpha} \\ f_\mathrm{b} = \mu_\mathrm{s}\cdot F_\mathrm{c}\cos\alpha = \mu_\mathrm{s}\left(\frac{1-\sin\varphi}{1+\sin\varphi}\right)\frac{\rho g_\mathrm{m} s^2 r_1 \mathrm{d}\theta\cos\alpha}{2\cos\alpha} \\ f_\mathrm{c} = \mu_\mathrm{s}\cdot G\cos\alpha = \mu_\mathrm{s}\frac{\rho g_\mathrm{m} s(r_0^2 - r_1^2)\mathrm{d}\theta\cos\alpha}{2\cos\alpha} \end{cases} \tag{5}$$

where $\mathrm{d}\theta$ is the circumference angle of the lunar regolith element, μ_s is the friction coefficient between the soil and the spiral flute, and μ_w is the friction coefficient between the soil and the wall of borehole. Assuming that the action by the active

Please cite this article in press as: Quan Q et al. Drilling load modeling and validation based on the filling rate of auger flute in planetary sampling, *Chin J Aeronaut* (2016), http://dx.doi.org/10.1016/j.cja.2016.05.003

earth pressure can convey soil upward, the deviation from the statics equilibrium is illustrated as follows:

$$f_w \geqslant f_b + f_c + G \cdot \sin\alpha \tag{6}$$

If the friction coefficient μ_s is equal to the friction coefficient μ_w, the following inequality can be acquired by connecting the above division and statics equilibrium inequality.

$$K_{ap} = \frac{s}{r_0 + r_1} \cdot \frac{1 - \sin\varphi}{1 + \sin\varphi} \cdot \frac{\tan(\varphi/2)}{\tan(\varphi/2) + \tan\alpha} \tag{7}$$

where K_{ap} is defined as the pushing coefficient of the soil's active earth pressure. If $K_{ap} > 1$, this means that the lunar regolith can be moved upward along the spiral flute by the active earth pressure. Otherwise, it cannot realize that the removal of the borehole cuttings cannot be achieved by the active pressure. As shown in Fig. 7, when the soil has a particular height, K_{ap} is smaller for a high internal angle of the lunar regolith and is always below 1. This can be explained that the active earth pressure based on the active earth pressure theory is negatively correlated with the soil's inner angle, which results in a smaller friction force to drive the soil to be removed up. Therefore, the pushing coefficient of the soil's active earth pressure K_{ap} becomes larger when the inner angle decreases.

According to the spiral transport theory, there exists a threshold of the auger's rotary speed n_t. When the auger's rotary speed n exceeds the speed threshold n_t, soil will be removed from the spiral flute fluently. In the following, a volume element of the lunar regolith element residing on the spiral flute is analyzed. Under a non-choking condition, the soil element will slide to the side of the hole wall due to the centrifugal force, as shown in Fig. 8(a), where the Cartesian coordinate system O-xyz for force and motion analysis is built on the surface of the spiral flute, F_{ce} is the centrifugal force, F_{fnf} is the friction force produced from the normal force F_{nf}, and $\bar{r}$ is the average radius of the lunar soil.

When the auger's rotary speed exceeds the threshold, soil will come into contact with the borehole wall and then the relative motion begins. Moreover, the direction of soil's absolute speed changes. As shown in Fig. 8(b), in this condition, v_r is the relative velocity, v_f is the following velocity by the rotary speed, v_p is the penetrating velocity, v_a is the absolute velocity, and β is the angle between the speed vector and the horizontal surface. The auger's rotary speed won't be too high, because it is restricted by the power supplied by the probe. Thus, the Coriolis force can be neglected in the force analysis. As shown

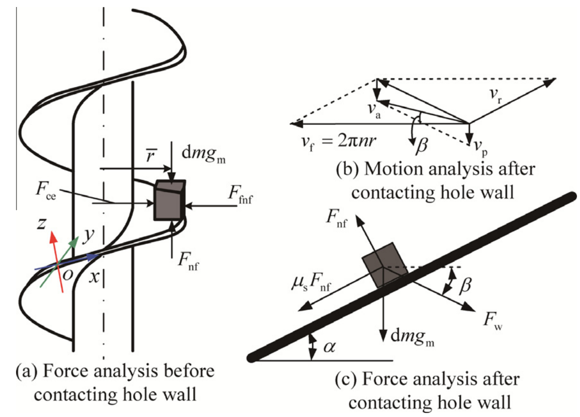

Fig. 8 Force analysis under the centrifugal force under a non-choking condition.

in Fig. 8(c), F_w changes the direction when the rotary speed exceeds the threshold. The force equilibrium equations of the lunar regolith are given as follows:

$$\begin{cases} \frac{\mu_w dm}{\bar{r}}(2\pi n\bar{r} - v_r\cos\alpha)^2\cos(\alpha+\beta) = dmg_m\sin\alpha + \mu_s F_n \\ F_n = dmg_m\cos\alpha + \frac{\mu_w dm}{\bar{r}}(2\pi n\bar{r} - v_r\cos\alpha)^2\sin(\alpha+\beta) \end{cases} \tag{8}$$

Based on the velocity triangle, the lunar regolith motion equations can be obtained as follows:

$$\begin{cases} v_r\sin\alpha - v_p = v_a\sin\beta \\ v_f - v_r\cos\alpha = v_a\cos\beta \end{cases} \tag{9}$$

Combining Eqs. (8) and (9), the lunar soil's helix angle and the relative velocity under a non-choking drilling condition will be acquired.

As long as the rotary speed of the auger is below the rotary speed threshold, the lunar regolith may not be conveyed by the centrifugal force. Meanwhile, the annular region between the coring tube and the auger's outer surface may be filled with the lunar regolith, producing additional stress. As shown in Fig. 9, a sector element of the lunar regolith filling in the flute ramp under a choking condition is analyzed. The Cartesian coordinate system O-xyz is built on the surface of the spiral flute.

Under a choking condition, the lunar soil element in the flute sustains the actions from the spiral blade, the wall of the borehole, and the cylindrical surface of the auger. By both actions (the thrust exerted by the bottom of the borehole and the friction exerted by the wall of the borehole), the lunar regolith element will be removed along with the spiral flute, in which the soil's motion is very similar to that under a non-choking condition. The force and torque equations are given as follows:

$$\begin{cases} F_p + F_{fw}\cos(\alpha+\beta) = G\sin\alpha + F_{fc} + F_{fs} + F_{fnf} \\ F_{ce} + F_{\sigma s} = F_{nw} \\ F_{nf} = G\cos\alpha + F_{fw}\sin(\alpha+\beta) + F_{\sigma c} \\ F_p\bar{r} + F_{fw}r_0\cos(\alpha+\beta) = F_{fs}\cdot r_1 + (F_{fc} + F_{fnf})\bar{r} + G\bar{r}\sin\alpha \end{cases} \tag{10}$$

where F_{ce} is the centrifugal force sustained of the lunar regolith, F_p is the thrust from the borehole, F_{nw} is the normal force on the wall of the borehole, F_{nf} is the normal force on the bot-

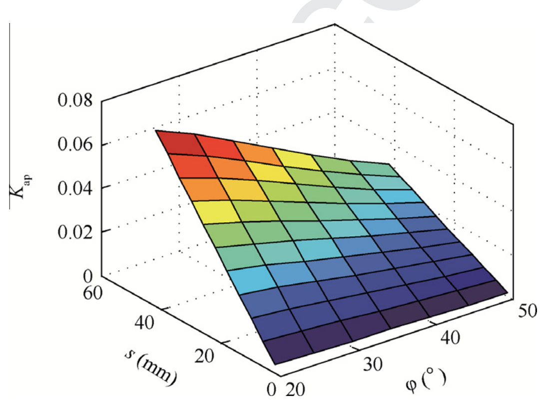

Fig. 7 Pushing coefficient of the soil's active earth pressure.

Please cite this article in press as: Quan Q et al. Drilling load modeling and validation based on the filling rate of auger flute in planetary sampling, *Chin J Aeronaut* (2016), http://dx.doi.org/10.1016/j.cja.2016.05.003

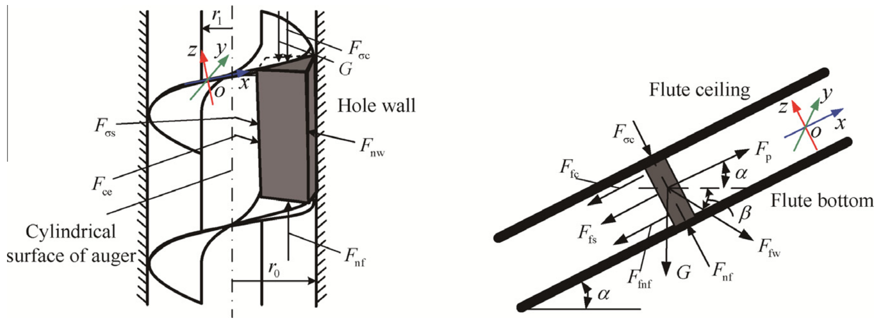

Fig. 9 Force analysis under additional stress under a choking condition.

tom of the flute, $F_{\sigma c}$ is the normal force on the ceiling of the flute by the additional stress, $F_{\sigma s}$ is the normal force on the cylindrical surface by the additional stress, F_{fc} is the friction force from the spiral flute's ceiling, F_{fs} is the friction force from the auger's cylindrical surface, and F_{fw} is the friction force from the hole wall.

For a stationary situation, the volume of cuttings produced must be equal to the volume of cuttings removed from the borehole. This can be expressed by the following equation:

$$v_r = \frac{v_p \pi (r_0^2 - r_2^2)}{(P - h_c)(r_0 - r_1)\cos\alpha} \tag{11}$$

Combining Eqs. (10) and (11), the additional stress under a choking condition can be acquired. As shown in Fig. 10, the additional stress of one lunar regolith simulant with an internal angle of 30° is calculated. From this figure, under a certain penetrating velocity, the additional stress increases when the rotary speed slightly decreases. This can be concluded that a higher rotary speed can relieve the choking condition. For a given rotary speed, the additional stress increases with the penetration velocity, showing that a low penetration velocity will be helpful for removing the lunar regolith.

3.3. Filling rate of auger flute (FRAF)

According to the above analysis of a lunar soil's conveyance mechanism, the filling condition of the spiral flute directly affects the auger's stress state. To acquire an accurate drilling model, the filling rate of auger flute (FRAF) K_f is proposed as:

$$K_f = \frac{S_1}{S_0} \times 100\% \tag{12}$$

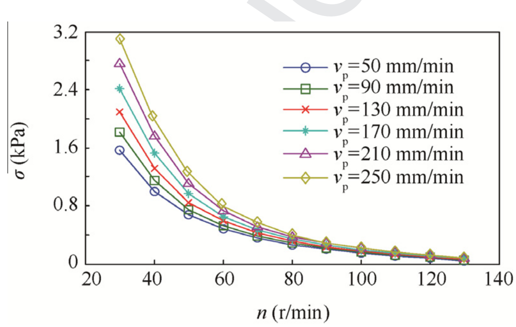

Fig. 10 Additional stress under a choking condition.

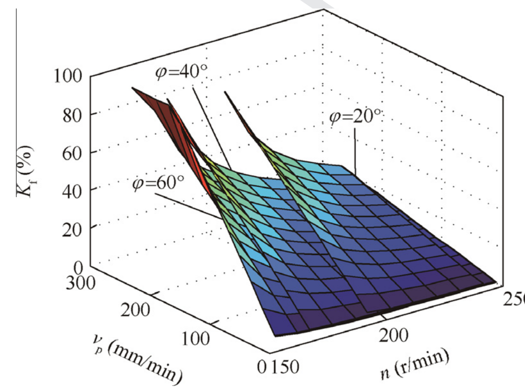

Fig. 11 FRAF K_f calculated in different conditions.

where S_0 is the transversal area of the auger flute and S_1 is the actual transversal area of the lunar soil removed by the auger flute. Based on the analysis of drilling conditions under different rotary speeds, drilling conditions can be divided into two typical cases. When $0 < n < n_t$, cuttings will be accumulated on the spiral flute until filling the flute, producing a choking condition. When $n > n_t$, cuttings will be removed by the centrifugal force, and the spiral flute will not be filled with cuttings, producing a non-choking condition.

Combining Eqs. (8), (9), and (12), K_f for different rotary speeds and penetration velocities can be obtained, as presented in Fig. 11. For a certain lunar regolith simulant, under the same rotary speed condition, K_f is closer to 100% when the penetration velocity is higher. Under the same penetration velocity, K_f is closer to 100% when the rotary speed is lower until $n < n_t$. Since the friction force from the wall of the borehole is the main driving force for removing cuttings, a lunar regolith with a larger internal angle is easier to be conveyed, and the corresponding K_f is smaller.

4. Modeling and validation

Based on the analysis of the conveyance mechanism in Section 3, a drilling load model describing a combination of the auger and the drill bit is presented now. Actually, according to the flexible tube coring method, there is no relative locomotion between the core and the sleeve. Compared with the drilling loads in the auger and the drill bit, the force or toque generated by the friction between the core and the sleeve may be very little, which could be neglected in the drilling

Please cite this article in press as: Quan Q et al. Drilling load modeling and validation based on the filling rate of auger flute in planetary sampling, *Chin J Aeronaut* (2016), http://dx.doi.org/10.1016/j.cja.2016.05.003

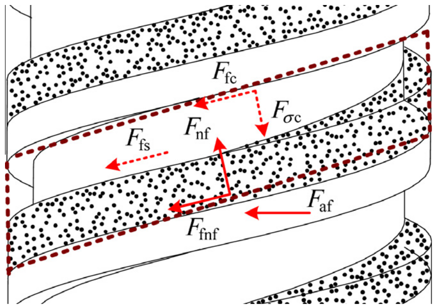

Fig. 12 Drilling loads on the auger in two conditions.

load's modeling. Since drilling conditions can be classified by the FRAF index, the models for the auger and the drill bit will firstly be considered separately, taking possible drilling conditions into account. The total drilling load can then be acquired by adding up these two contributions.

4.1. Drilling load modeling

According to the motion and force analysis of lunar regolith presented in Section 3, the drilling loads on the auger mainly contain the following six parts. As shown in Fig. 12, F_{af} is the friction force acting on the spiral blade. Since the lunar regolith simulant is compressed to keep homogenous, the drilled borehole can be held well in the course of a drilling operation and the wall of the borehole will be rather smooth. Hence, for calculating drilling loads, the friction force on the spiral blade F_{af} can be neglected.

Under a non-choking condition, the drilling loads on the auger mainly contain the supporting force and the force on the bottom of the spiral flute. Deploying the spiral line, the deploying angle of the lunar regolith at a certain height h can be acquired as $\chi = h/(\bar{r}\sin\alpha)$. In a non-choking condition, the rotary torque and penetration force that drill tool sustains can be obtained as follows:

$$\begin{cases} T_{a1} = \int_0^{\chi} N_t \cdot (F_{fnf}\cos\alpha + F_{nf}\sin\alpha)\bar{r}\,\mathrm{d}\theta \\ F_{pa1} = \int_0^{\chi} N_t \cdot (F_{fnf}\sin\alpha - F_{nf}\cos\alpha)\,\mathrm{d}\theta \end{cases} \tag{13}$$

where N_t is the number of the auger's spiral line. Combining Eqs. (12) and (13) together, the drilling loads on the auger in a non-choking condition can be acquired.

Under a choking condition, the cuttings in the spiral flute will be extruded and conveyed. In this drilling condition, the auger not only sustains the supporting force and the force on the bottom of the flute, but also sustains the supporting force and the force on the flute ceiling as well as the force on the cylindrical surface. At a certain height, the rotary torque and penetration force sustained by the drill tool can be calculated as follows:

$$\begin{cases} T_{a2} = \int_0^{\chi} N_t \cdot [(F_{fnf} + F_{fc} + F_{fs})\cos\alpha + (F_{nf} - F_{\sigma c})\sin\alpha]\bar{r}\,\mathrm{d}\theta \\ F_{pa2} = \int_0^{\chi} N_t \cdot [(F_{fnf} + F_{fc} + F_{fs})\sin\alpha + (F_{\sigma c} - F_{nf})\cos\alpha]\,\mathrm{d}\theta \end{cases} \tag{14}$$

Since the filling rate of auger flute $K_f = 1$ in a choking condition, combining Eqs. (10), (11), and (14), the drilling loads on the auger in a choking condition can be acquired.

According to the difference in failure mechanism, the lunar regolith surrounding the drill bit can be divided into two parts: the cutting area and the accumulation area.[27] The lunar regolith in the cutting area mainly sustains the shearing damage by the cutting blade, and the cuttings in the accumulation area are mainly removed by the wall of the borehole. As shown in Fig. 13, according to the difference in boundary constraint, the accumulation area can be divided into accumulation zone A_1 and zone B_1.

Accumulation zone A_1, forming a triangular wedge *AFQ-BGP*, is connected with the cuttings in the spiral flute. Accumulation zone B_1 is restricted by the transition plane and forms a trapezoidal shape wedge *BSMJ-CHNK*.

According to the morphological analysis of the soil in the drill bit, the drilling loads on the drill bit mainly contain the following nine contributions, as shown in Fig. 14. Compared with the accumulation area, the area of cutting is too small, so the cohesion force F_{cc} and the friction force F_{cf} in the cutting area are neglected. The specific components of the drilling loads on the drill bit are given in Table 2.

Under a non-choking drilling condition, the cuttings in the accumulation area only sustain a tangential load. This implies that the penetration force in the accumulation area $F_{pa} = 0$. The drilling loads in a non-choking drilling condition are mainly caused by F_{af1} and the cohesion force F_{ac1} between cuttings in the accumulation area and the wall of the borehole, F_{af2} and the cohesion force F_{ac2}, and the Rankine passive earth pressure F_{cp}. Each drilling load component, the rotary torque, and the penetration force are as follows:

$$\begin{cases} T_{ac1} = N_t F_{ac1} r_0 = N_t l_a^2 \tan\theta \cdot c_a r_0/2 \\ T_{af1} = N_t F_{af1} r_0 = N_t \tan\varphi \cdot \rho V \omega^2 r_0^2 \\ T_{ac2} = N_t \int_{r_2}^{r_0} F_{ac2} r\,\mathrm{d}r = N_t \int_{r_2}^{r_0} l_a c_a r\,\mathrm{d}r \\ T_{af2} = N_t \int_{r_2}^{r_0} F_{af_2} r\,\mathrm{d}r = N_t \int_{r_2}^{r_0} \frac{W_a}{r_0 - r_2} \tan\varphi r\,\mathrm{d}r \\ T_{ba1} = T_{af1} + T_{ac1} + T_{af2} + T_{ac2} \\ T_{bc1} = N_t F_{cp1} \cos\varphi (r_0^2 - r_2^2)/2 \\ T_{b1} = T_{ba1} + T_{bc1} \\ F_{pb1} = F_{ba1} + F_{bc1} = N_t F_{cp1} \sin\varphi (r_0 - r_2) \end{cases} \tag{15}$$

where c_a is the cohesion of the cuttings in the accumulation area, W_a is the weight of the cuttings in the accumulation area, and l_a is the length of the bottom of the accumulation area. Combining Eqs. (11) and (15), drilling loads on the drill bit in a non-choking condition can be acquired.

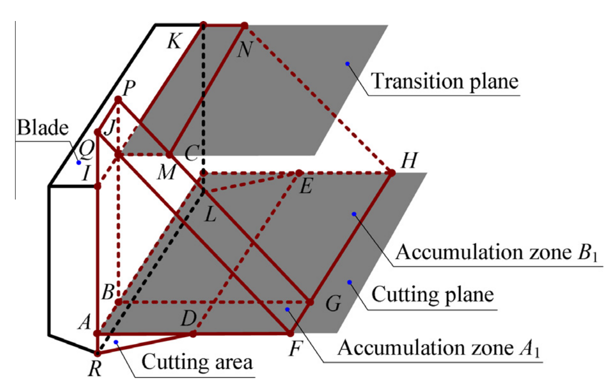

Fig. 13 Morphological analysis of the soil surrounding the drill bit.

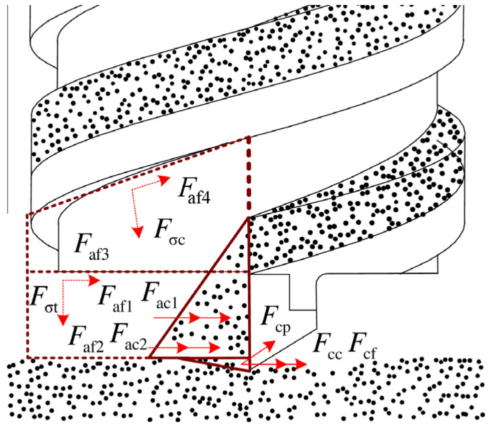

Fig. 14 Drilling loads on the drill bit in two conditions.

Table 2 Components of the drilling load on the drill bit.

Component of drilling load	Symbol
Friction force between cuttings and the wall of borehole	F_{af1}
Cohesion force between cuttings and the wall of borehole	F_{ac1}
Friction force between cuttings and the bottom of borehole	F_{af2}
Cohesion force between cuttings and the bottom of borehole	F_{ac2}
Rankine passive earth pressure	F_{cp}
Normal force on the transition plane by the additional stress	$F_{\sigma t}$
Friction force on the transition plane by the additional stress	F_{af3}
Normal force on the ceiling of spiral flute by the additional stress	$F_{\sigma c}$
Friction force on the ceiling of spiral flute by the additional stress	F_{af4}

In a choking drilling condition, cuttings in the accumulation area bear the action by the additional stress and are removed by the extruding action. The shape of the accumulation area is a closed wedge, where the accumulation angle $\theta = \alpha$ and the filling rate of auger flute $K_f = 1$. In addition to the drilling loads in a non-choking condition, the drill bit also sustains the supporting forces $F_{\sigma t}$ and $F_{\sigma c}$, as well as the friction forces F_{af3} and F_{af4} from the transition plane and the ceiling plane of the spiral flute, respectively. Each component of the drilling loads, the rotary torque, and the penetration force in a choking condition are as follows:

$$\begin{cases} T_{ba2} = N_t(F_{af1} + F_{af1})r_0 + N_t(F_{af2} + F_{ac2} + F_{af3} + F_{\sigma c}\sin\alpha + F_{af4}\cos\alpha)\bar{r} \\ T_{bc2} = N_t F_{cp2}(r_0^2 - r_2^2)\cos\varphi/2 \\ T_{b2} = T_{ba2} + T_{bc2} \\ F_{pb2} = N_t(W_a + F_{\sigma c} + F_{\sigma c}\cos\alpha - F_{af4}\sin\alpha) + N_t F_{cp}(r_0 - r_2)\sin\varphi \end{cases} \tag{16}$$

Combining Eqs. (10), (11), and (16), the drilling loads on the drill bit in a choking condition can be acquired. In summary, by evaluating the filling rate of auger flute (FRAF) index, the piercing process with different drilling parameters can be classified as either a non-choking condition or a choking condition. After calculating the drilling loads on the auger and the drill bit respectively, the total drilling load is obtained by adding up the two components.

4.2. Model validation

When conducting the drilling and coring experiments, a flexible tube of 130-mm length is positioned in the hollow auger, as shown in Fig. 15. Once the drill bit is in contact with the soil surface, one tip of the dragging wire is fixed at a point on the test platform, while the other tip is connected to the starting point of the flexible tube and is kept in a tense state.[5] When the desired drilling depth is reached, the sealing tip at the end of the flexible tube is activated to collect the coring sample into the closed space inside the flexible tube. To distinguish the cuttings removed with those in the spiral flute, an isolation plate was mounted on the surface of the lunar regolith passing through the auger.

Drilling parameters in the drilling and coring experiments are given as follows: rotary speed n = 40, 80, 120, 160, 200, 240 r/min and penetrating velocity v_p = 40, 80, 120, 200, 240 mm/min. According to the 6×6 matrix, repeated tests are conducted. In the experiments, drilling loads are monitored, not exceeding the maximum drilling loads that test platform can sustain. The test results on the HIT-LS1# lunar regolith simulant are shown in the above figure.

According to the discussion in Section 3, the FRAF is applied in our drilling loads model to determine drilling conditions. To verify the correctness of the proposed FRAF concept, verification tests should be carried out. Neglecting the effect on the soil's density by the drilling depth, the FRAF K_f can be equivalent to the mass ratio between the actual mass in the spiral flute M_2 and the theoretical one M_t, as shown in Eq. (17):

$$K_f = \frac{S_1}{S_0} \times 100\% = \frac{M_2}{M_t} \times 100\% \tag{17}$$

During the drilling process, three types of lunar regolith are produced: accumulation soil $M_a(H)$, soil in the spiral flute $M_s(H)$, and coring soil $M_c(H)$. According to the conservation of mass, the following equation can be obtained:

$$M_t(H) = M_a(H) + M_s(H) + M_c(H) \tag{18}$$

Since the soil in the spiral flute is in a confined space, its mass cannot be measured accurately. Herein, to a certain depth H, $M_s(H)$ can be indirectly acquired by measuring the mass of the accumulation soil $M_a(H)$ and that of coring soil $M_c(H)$ separately, as shown in Fig. 16.

Using the mechanical parameters of the lunar regolith simulant in Eq. (12), a comparison of results between the theoretically calculated FRAF and the FRAF obtained from the experiments can be made. The results are shown in Fig. 17. This comparison indicates that the calculated FRAF coincides with the test results quite well. With the same rotary speed, the FRAF increases with the penetration velocity and at a higher velocity, the FRAF changes significantly. The FRAF becomes smaller when the rotation speed is higher. At a low rotation speed and a high penetration velocity, the FRAF is always equal to 1, which means that the drill tool gets blocked in this drilling parameters regime. At a high rotary speed, the FRAF is constantly less than 1, meaning that the drill tool is not

Please cite this article in press as: Quan Q et al. Drilling load modeling and validation based on the filling rate of auger flute in planetary sampling, *Chin J Aeronaut* (2016), http://dx.doi.org/10.1016/j.cja.2016.05.003

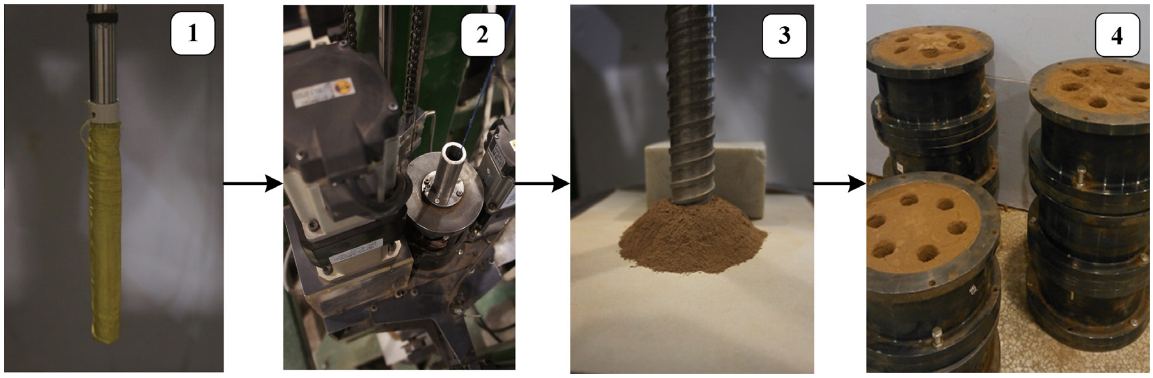

Fig. 15 Working process of drilling and coring experiments.

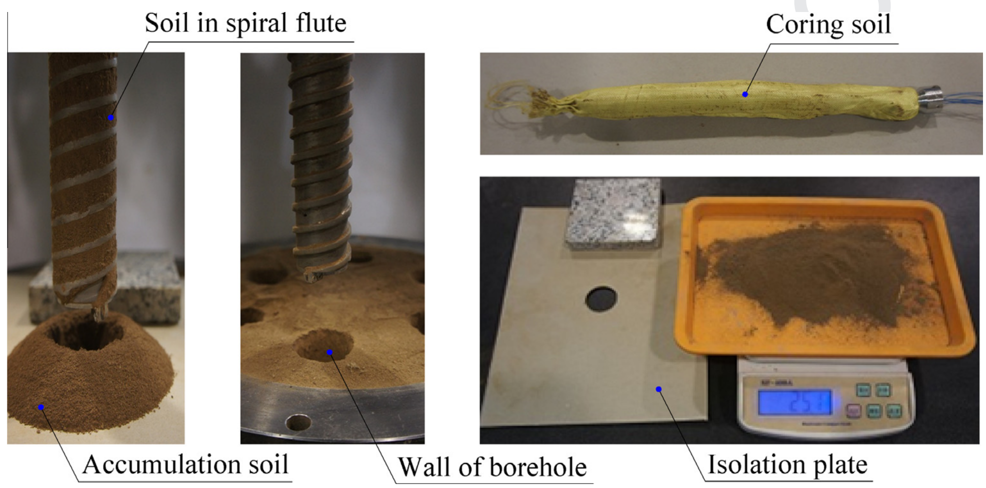

Fig. 16 Working process of drilling and coring tests.

blocked and thus the cuttings in the spiral flute are removed fluently. The experimental results presented above show that the proposed FRAF concept can describe the drilling conditions in different drilling parameter ranges quite well and thus can be used to establish the drilling load model.

In addition to the masses of the accumulation soil and the coring soil, drilling loads are also acquired by the drilling and coring process. The mechanical parameters of the lunar regolith simulant in our drilling load model and the comparison results between theoretical and experimental rotary torques are shown in Fig. 18.

From the rotary torque comparison results shown in Fig. 18, the calculated rotary torque obtained from the theoretical model also coincides well with the test results. Under the same rotary speed, the rotary torque T increases with the penetration velocity significantly. At a high penetration velocity, the rotary torque changes significantly, and at a low penetration velocity, the growth of the rotary torque becomes more moderate. This can be explained by the fact that a high penetration velocity leads to increases of the cutting volume and the FRAF, causing more easily a blocking of the drilling tool. Under the same penetration velocity, the rotary torque T becomes smaller when the rotary speed is higher. At a high rotary speed, the rotary torque changes significantly, and at a low rotary speed, the growth of the rotary torque becomes moderate. When the penetration velocity v_p = 120 mm/min, the rotary torque reaches 34 N m, almost the maximum drilling load that test platform can sustain. As shown in Fig. 18 (f), a high rotary speed results in an increase of the centrifugal force, so cuttings can be removed fluently and the corresponding rotary torque is less than 1 Nm.

5. Drilling parameters optimization

The goal of drilling load modeling is to acquire suitable drilling parameters for different drilling conditions and thereby to improve the sampling drill's environmental adaptability. Based on the drilling model validated in Section 4, the drilling load in one simulant was obtained. According to the lunar exploration requirements, drilling parameters of this simulant can be optimized reasonably under limited drilling power, penetration force, etc.

5.1. Optimization indexes

Due to limited in-orbit weight and power supply, a lunar sample return mission has several requirement indices. These can be divided into safety index and functional index. The safety index is proposed to confirm the mission's reliability and must

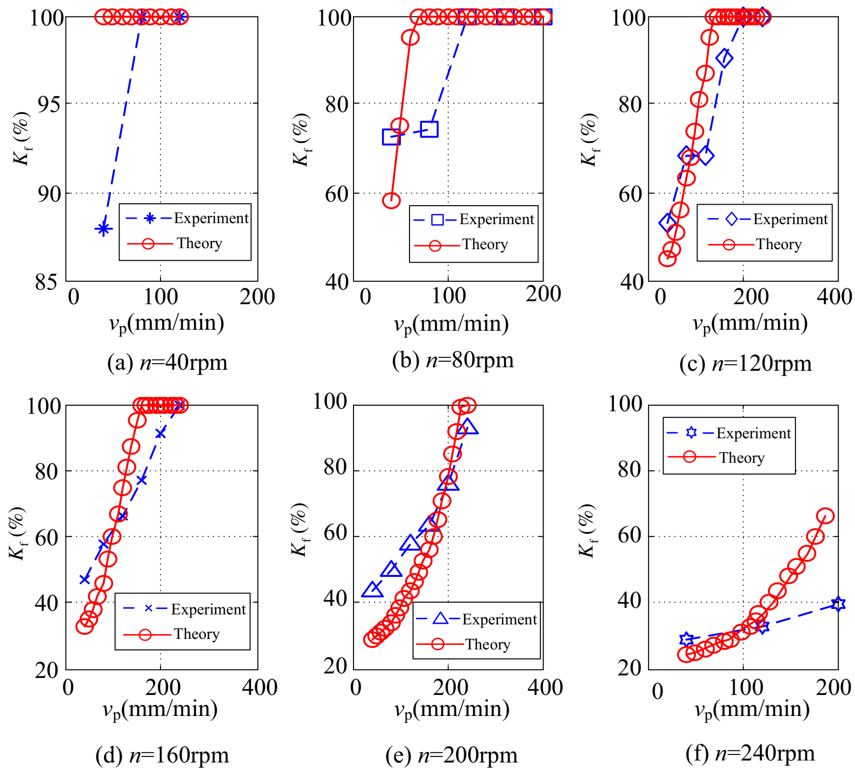

Fig. 17 FRARs in theory and experiment.

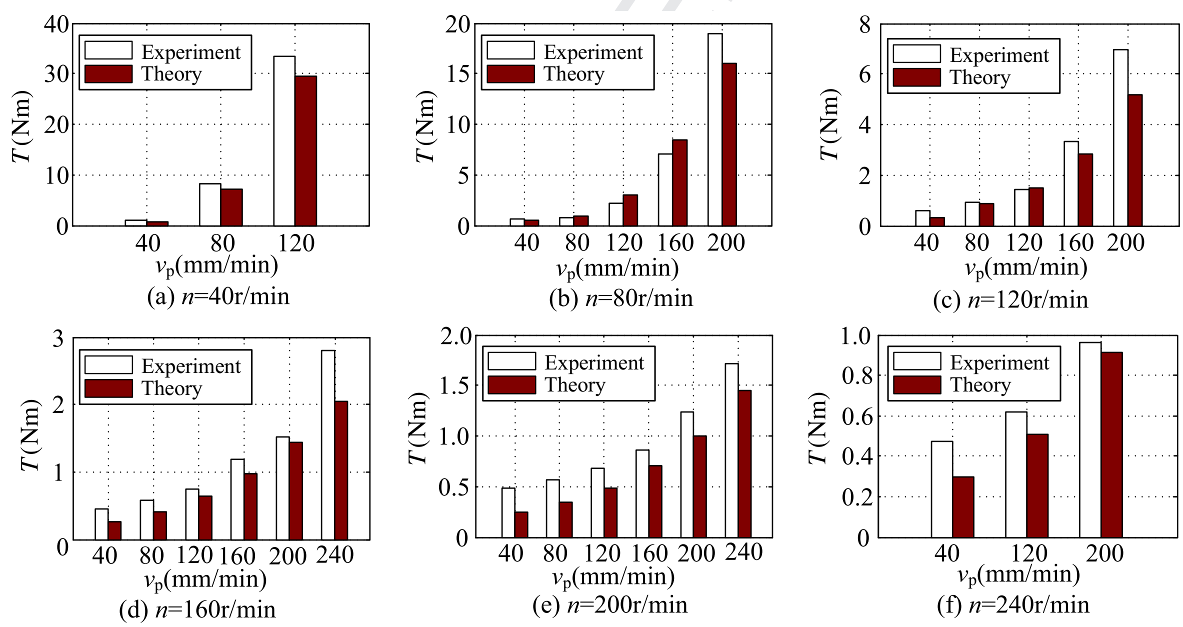

Fig. 18 Drilling loads in theory and experiment.

be obeyed. The functional index indicates to which extent the system has been optimized to fulfill its foreseen task effectively. Suitable drilling parameters should satisfy the requirements of both the safety index and the functional index.

Restricted by the driving capacity of the rotary motor, the rotary torque T should not be more than 30 Nm. By the lander weight constraint, the penetration force F_p should be less than 800 N. By the probe's power supply capacity constraint, the drilling power P_d and the energy W_d are required to be less than 100 W and 50 W h, respectively. Since the main goal of lunar drilling and coring is to acquire lunar regolith, the sampling rate K should not be too low. Herein, the sampling rate K is required to be more than 90%. According to experimental research on the ground, overlong drilling time will lead to a decrease of the sampling rate.[28] Therefore, the total drilling time T_t is restricted to be 0.5 h for a 2-m depth and the corresponding penetrating velocity v_p should be more than 80 mm/min.

5.2. Optimization method

Since the intended landing spot in China's future lunar exploration mission is the rainbow bay area on the Moon, the lunar regolith acquired by the Apollo15 mission at the "Hadley Rile" is chosen as the drilling formation.[29]. Taking the mechanical parameters of this lunar regolith into the drilling load model established in Section 4, the corresponding rotary torque, penetrating force, drilling power, and drilling energy are acquired, as shown in Fig. 19.

The relationship between the sampling rate K and the ratio of v_p to n was discussed in former experimental research.[28]. The rotary speed n and the penetration velocity v_p are restricted by the above optimization indexes, as shown in Fig. 20. The black shaded region in Fig. 20 corresponds to the drilling parameter values meeting the requirements of the tasks.

According to the principle of least energy consumption in metal cutting theory, there exists an appropriate combination of drilling parameters (n_o, v_{po}, f_{pero}) minimizing the drilling total energy, as shown in the following equation:[30]

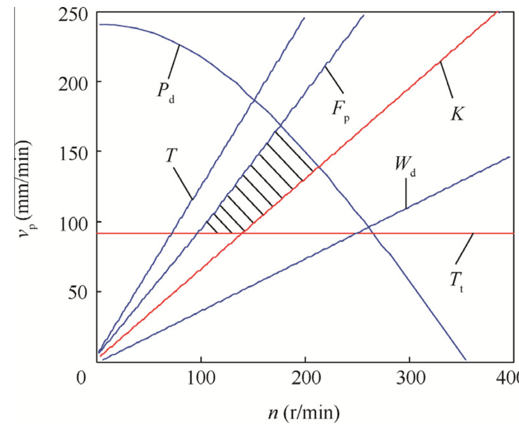

Fig. 20 Range of suitable drilling parameters.

$$\begin{cases} W_d = P_d \cdot T \\ W_{dmin} = W_d(n_o, v_{po}, T_o, F_{po}, T_{to}) \end{cases} \quad (19)$$

where n_o is the optimized rotary speed, v_{po} is the optimized penetrating velocity, T_o is the optimized rotary torque, F_{po} is the optimized penetrating force, T_{to} is the optimized drilling total time, and W_{dmin} is the optimized drilling energy. Using the mechanical parameters of lunar regolith in the above equation, the optimized drilling parameters are as follows: rotary

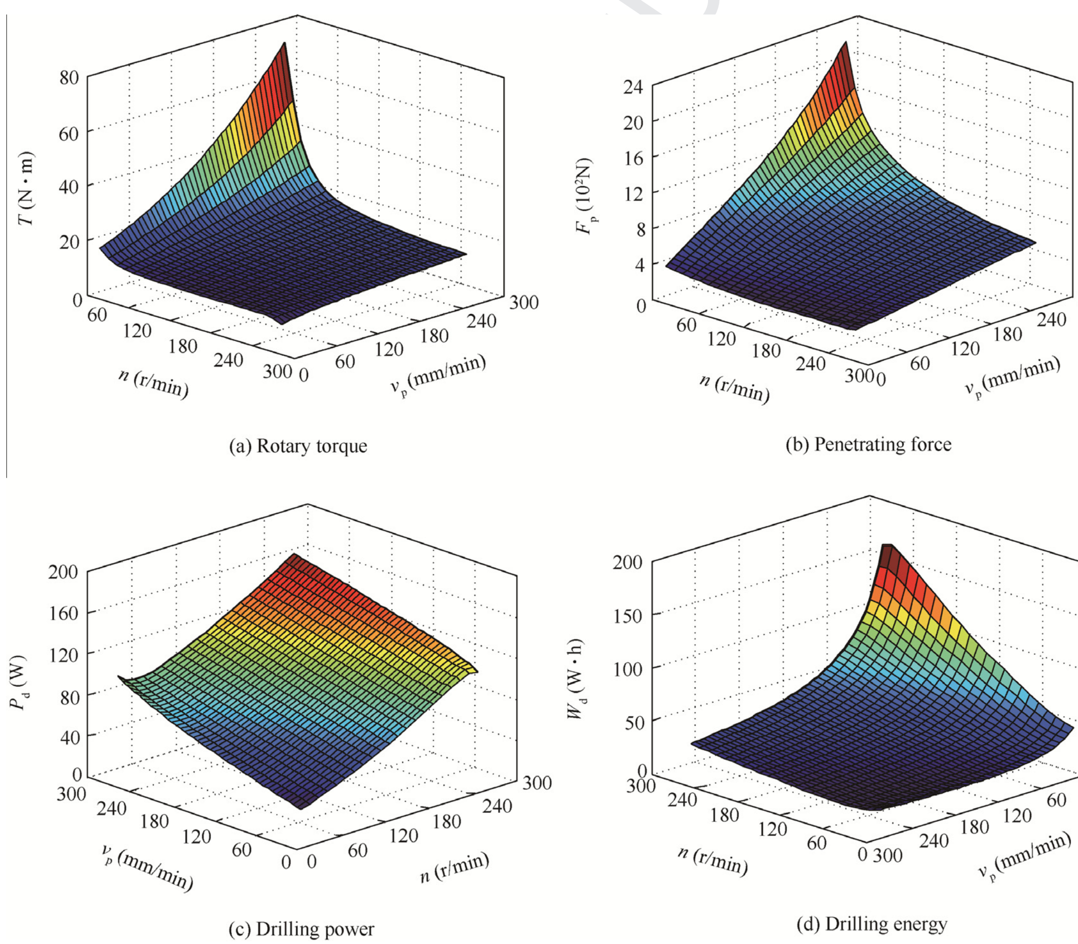

Fig. 19 Predicted drilling loads based on the established drilling load model.

speed $n_o = 85$ r/min and penetration velocity $v_{po} = 80$ mm/min. The minimum drilling energy for drilling a 2-m depth $W_o = 38.56$ Wh, and the optimized coring rate $K_o = 94.6\%$, meeting all the requirements for the future task.

6. Conclusions

This paper analyzes the failure mode and conveyance state of the lunar regolith. The filling rate of auger flute (FRAF) is proposed to classify drilling conditions into two typical conditions: non-choking and choking conditions. Based on the spiral transport theory, a drilling load model combing the loads on the auger and the drill bit has been established. Experiments in one typical lunar regolith simulant HIT-LS1# soil under different combinations of drilling parameters indicate that this drilling load model based on the FRAF coincides with the test results reasonably well. Based on this drilling load model and optimization indices analyzed, drilling parameters of the lunar regolith simulant can be optimized by using the principle of least energy consumption.

Acknowledgments

The authors thank the supports by the National Natural Science Foundation of China (No. 61403106, No. 51575122), Program of Introducing Talents of Discipline to Universities (No. B07018) of China, and Fundamental Research Funds for the Central Universities (No. HIT.NSRIF.2014051) of China.

Appendix A. Supplementary material

Supplementary data associated with this article can be found, in the online version, at http://dx.doi.org/10.1016/j.cja.2016.05.003.

References

1. Ronca LB. An introduction to the geology of the moon. *Proc Geol Assoc* 1966;**77**(1):101–25.
2. Ouyang ZY, Li CL, Zou YL, Liu JZ, Liu JJM. The primary science result from the chang'e-1 probe. *Sci China Earth Sci* 2010;**40**(3):261–80.
3. Bar-Cohen Y, Zacny K. *Drilling in extreme environment: penetration and sampling on earth and other planets*. Weinheim: Wiley-VCH; 2009. p. 1–30.
4. Zacny K, Bar-Cohen Y. Drilling and excavation for construction and in-situ resource utilization. In: Badescu V, editor. *Mars prospective energy and material resources*. Berlin: Springer-Verlag; 2009. p. 431–59.
5. Quan QQ, Tang JY, Jiang SY, Li H, Li SC, Deng ZQ, et al. Control system for a drilling & coring device in lunar exploration. *Proc of the IEEE international conference on information and automation, 2013 Aug. 26–28; Yinchuan, China*. Piscataway, NJ: IEEE Press; 2013. p. 79–84.
6. Shi XM, Deng ZQ, Quan QQ, Tang DW, Hou XY, Jiang SY. Development of a drilling and coring test-bed for lunar subsurface exploration and preliminary experiments. *Chin J Mech Eng* 2014;**27**(4):673–82.
7. Heiken GH, Vaniman DT, French BM. *Lunar sourcebook: a user's guide to the moon*. Paris: Cambridge University Press; 1991. p. 285–356.
8. Lian Y. *Inversion of composition and analysis of structure in the lunar subsurface from chang'e microwave data [dissertation]*. Changchun: Jilin University; 2014.
9. Shi XM, Jie DG, Quan QQ, Tang DW, Jiang SY, Deng ZQ. Experimental research on lunar soil simulant drilling load analysis. *Chin J Astronaut* 2014;**35**(6):648–56.
10. Zhong Z. *Theoretical and experimental analysis of the compaction process in a tapered screw press [dissertation]*. Newcastle: The University of Newcastle upon Tyne; 1991.
11. Robert A, Willis A. Performance of grain augers. *Proc of the institute of mechanical engineers*, vol. 176, 8. p. 165–94.
12. Zacny K, Quayle MC, Cooper GA. Laboratory drilling under martian conditions yields unexpected results. *J. Geophys. Res.* 2004;**109**(1):E07S16.
13. Zacny K. *Mars drilling- an investigation and development of techniques for drilling exploratory boreholes on mars [dissertation]*. Berkeley: University of California, Berkeley; 2005.
14. Tian Y, Deng ZQ, Tang DW, Jiang SY, Hou XY. Structure parameters optimization and simulation experiment of auger in lunar soil drilling-sampling device. *Chin J Mech Eng* 2012;**48**(23):10–5.
15. Deng ZQ, Tian Y, Tang DW, Jiang SY, Quan QQ, Xiao H. Research on new structure coring bit for extraterrestrial bodies exploration. *Chin J Mech Eng* 2013;**49**(19):104–10.
16. Vrettos C. Shear strength investigation for a class of extraterrestrial analogue soils. *J Geotech Geoenviron Eng* 2012;**138**(4):508–15.
17. Williams DE. *To a rock moon: a geologist's history of lunar exploration*. Tucson: University of Arizona Press; 1994. p. 137–49.
18. Butler JC, King EA. Analysis of grain size frequency distributions of lunar fines*Proc of 5th lunar planet science conference*. p. 829–41.
19. Mitchell JK, Bromwell LG, Carrier III NC, Costes NC, Scott RF. Soil mechanical properties at the apollo 14 site. *J. Geophys. Res.* 1972;**77**(29):5641–64.
20. Mitchell JK, Houston WH, Scott RF, Bromwell L. Mechanical properties of lunar soil: density, porosity, cohesion and angle of internal. *Proc of the third lunar science conference*. p. 3235–53.
21. Yan T. *Rock and soil drilling technology*. Wuhan: Chinese University of Geoscience Press; 2001. p. 65–92.
22. Shi XM, Tang DW, Quan QQ, Jiang SY, Hou XY, Deng ZQ. Development of a drilling and coring test-bed for lunar subsurface exploration. *Proc of the IEEE international conference on robotics and biomimetics, 2013 Dec. 12–14; Shenzhen, China*. Piscataway, NJ: IEEE Press; 2013. p. 2124–9.
23. Quan QQ, Li P, Jiang SY, Hou XY, Tang DW, Deng ZQ, et al. Development of a rotary-percussive drilling mechanism (rpdm) *Proc of the IEEE international conference on robotics and biomimetics, 2012 Dec. 11–14; Guangzhou, China*. Piscataway, NJ: IEEE Press; 2012. p. 950–5.
24. Ross I, Isaace G. Capacity of enclosed screw conveyors handling granular materials. *Trans Am Soc Agric Eng* 1961;**4**(1):97–104.
25. Mellor M. *Mechanics of cuttings and boring*. USA Army Cold Regions Research and Engineering Laboratory; 1981, Report.
26. Collins JA. *Failure of materials in mechanical design: analysis, prediction, prevention*. New York: Wiley; 1993. p. 105–85.
27. Tang JY. *Research on drilling strategy of lunar drilling and coring based on real-time recognition of drillability [dissertation]*. Harbin: Harbin Institute of Technology; 2014.
28. Shi XM, Quan QQ, Tang DW, Jiang SY, Hou XY, Deng ZQ. Experimental research on drilling and sampling of lunar soil simulant. *Appl Mech Mater* 2012;**233**(1):218–23.
29. Richard WO, David MH. *Apollo the definitive sourcebook*. Chi Chester: Springer; 2006. p. 425–69.
30. Shi H. *Metal cutting theory and practical new perspective*. Wuhan: Huazhong University of Science and Technology Press; 2003. p. 201–26.

Quan Qiquan is an associate professor in the School of Mechatronics Engineering at Harbin Institute of Technology, Harbin, China. He

received his B.S. and M.S. degrees from Harbin Institute of Technology in 2005 and 2007, respectively, and his Ph.D. degree from Ritsumeikan University, Japan, in 2010. His main research interests include automated planetary sampling, ultrasonic levitation, and an orbit and ground test for space mechanism.

Tang Junyue is a Ph.D. candidate in the School of Mechatronics Engineering at Harbin Institute of Technology, Harbin, China. He received his M.S. degree from HIT in 2014. His current research area is automated planetary sampling.

Yuan Fengpei is an undergraduate student in the School of Mechatronics Engineering at Harbin Institute of Technology, Harbin, China. She visited Seoul National University, Korea, during her junior year from 2014 to 2015. She currently works in designing a planetary drilling and coring test-bed for experiments.

Jiang Shengyuan is a professor in the School of Mechatronics Engineering at Harbin Institute of Technology, Harbin, China. He received his M.S. and Ph.D. degrees from the HIT in 1998 and 2001, respectively. His current research interests include automated planetary sampling, and space mechanism.

Deng Zongquan is a professor in the School of Mechatronics Engineering at Harbin Institute of Technology, Harbin, China. His current research interests include automated planetary sampling, planetary rover, and space mechanism.